Green Chemistry

Accepted Manuscript

ROYAL SOCIETY OF CHEMISTRY

www.rsc.org/greenchem

Cite this: DOI: 10.1039/c0xx00000x

www.rsc.org/xxxxxx

ARTICLE TYPE

Biomass-Derived Porous Carbon Materials with Sulfur and Nitrogen Dual-Doping for Energy Storage

Guiyin Xu, Jinpeng Han, Bing Ding, Ping Nie, Jin Pan, Hui Dou, Hongsen Li and Xiaogang Zhang*

Received (in XXX, XXX) Xth XXXXXXXXX 20XX, Accepted Xth XXXXXXXXX 20XX

DOI: 10.1039/b000000x

Nowadays, energy shortage is a serious problem in our society. The recovery of biomass is significantly important for alleviating the burden on strained energy resources. Broad beans, abundant in amino-acids and vitamins, are heavily cultivated around the world. However, a great quantity of by-product, the shell of broad beans, is abandoned and pollutes the environment from the sintering. Herein, we report the synthesis of sulfur and nitrogen dual-doping porous carbon materials for the electrode materials of energy storage devices *via* carbonizing the shell of broad beans with a chemical activation. The specific capacitance of the as-prepared porous carbon material is as high as 202 F g^{-1} with a superior cycling performance for electric double layer capacitors at a current density of 0.5 A g^{-1}. Moreover, it also shows stable performance for lithium-ion batteries and sodium-ion batteries, which suggests it has promising potential for wide applications in the energy storage devices.

Introduction

Biomass is an available nature resource.[1, 2] If it is sintered, greenhouse effect, brume and other malignant environment damages will bring in. Therefore, the conversion of biomass is becoming the worldwide research hotspot. Broad beans are a crop species for human food. However, tons of the shell of broad beans (SB), by-product of broad beans, are produced every year. Although SB is traditionally fed to animals, there are still a large quantity to be sintered or abandoned. As a legume, SB is rich in amino-acids and vitamins.[3] Therefore, SB can be transformed to carbon materials with heteroatom doping by calcining it in an inert gas (**Figure 1**), which is significantly important for the sustainable development of society. Heteroatom-doped carbon materials have a wide range of applications, such as catalysis,[4, 5] biosensing,[6] bioimaging,[7] energy conversion,[8, 9] energy storage systems,[10-12] and other electronic devices.[13, 14] Among the current energy storage options, electric double layer capacitors (EDLCs), lithium-ion batteries (LIBs), and sodium-ion batteries (SIBs) are paid much attention due to their high power and energy density.[15-20]

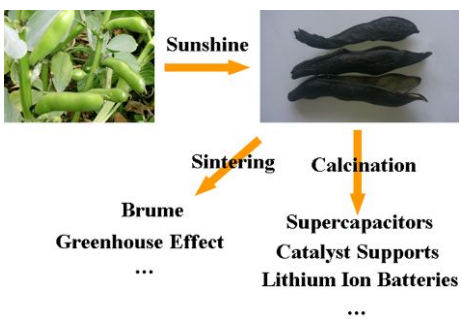

Figure 1. Illustration for the different process modes of SB

In recent years, porous carbon materials are promising candidates for EDLCs and LIBs because of their high electric conductivity, large specific area, and easy availability.[21-23] There have been many reports about porous carbon materials, for instance, mesoporous carbon spheres,[24] reduced graphene oxide,[25, 26] and carbide-derived carbon thin film[27] as electrodes for EDLCs and carbon nanotube-graphene,[28] hollow carbon capsules,[29] and hollow carbon nanospheres[30] as anodes for LIBs. In the past, a lot of porous carbon materials were prepared by soft or hard template synthesis method,[16, 17, 31-33] in which the synthesis process was complex and the yield was often low. Moreover, the further modification optimization of porous carbon materials is quite meaningful for practical application.[12, 34] Porous carbon materials with sulfur or nitrogen doping can enhance the specific capacitance for EDLCs[35, 36] and improve the specific capacity or rate capability for LIBs/ SIBs.[8, 37-39]

Combining with the increasing environmental problems caused by sintering SB, a motivation is proposed of employing the waste by-product to prepare porous carbon materials for energy storage applications. Herein, we present porous carbon materials with heteroatom doping for energy storage devices through the carbonization of the shell of broad beans (CSB) in an inert gas and the further chemical activation (ACSB). Compared to the previous methods of synthesizing porous heteroatom-doped carbon materials, our work has several advantages as follow: (1) SB is resource-rich and sustainable resulting in a low cost; (2) SB abundant in nitrogen and sulfur sources is an ideal precursor for sulfur and nitrogen dual-doping carbon materials; (3) The overall synthesis process is simple and easy handling, which is suitable for the industrial production; (4) The obtained porous carbon material (ACSB) with large specific surface area, unique pore-size distribution, sulfur-nitrogen dual-doping, and high electrical

conductivity could been widely applied in energy storage devices. Simultaneously, the electrochemical results demonstrate the as-prepared carbon materials are promising candidates for energy storage devices.

Results and discussion

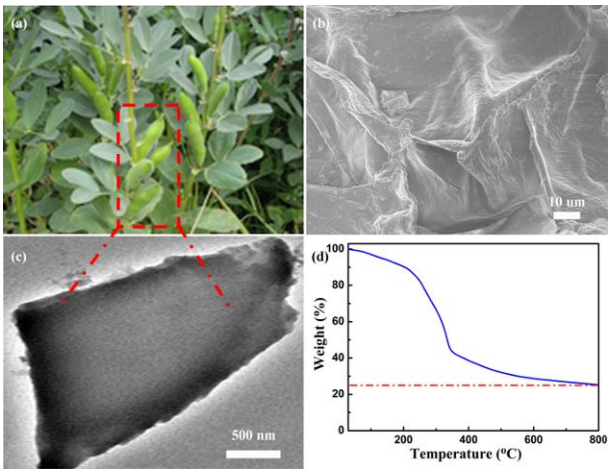

Figure 2. (a) Digital photograph, (b) SEM image, and (c) TEM image of SB, (d) TG curve of CSB from the pyrolysis of SB under an inert atmosphere.

In the pursuit of environmental protection for the social sustainable development and low cost for energy storage devices, SB abundant in renewable biomaterial (**Figure 2a**) arouses our great interests. More importantly, SB is rich in protein, which is mainly composed of carbon, hydrogen, oxygen, nitrogen, and sulfur. Therefore, SB is a promising precursor for synthesizing carbon materials with heteroatom-doping. Interestingly, the morphology of SB is like graphene as shown in **Figure 2b**, which displays a wrinkled laminar structure similar to the previous reports of graphene.[25, 40] Transmission electron microscopy (TEM) image demonstrates the laminar structure of SB (**Figure 2c**). Meanwhile, thermal gravimetric (TG) analysis was carried out to investigate the carbonization process of SB in inert atmosphere. The TG curve shows a distinct weight loss stage from around 200 to 600 °C (**Figure 2d**). The weight loss is primarily due to the evaporation of H_2O, CO_2 and CO, resulting from the escape of H and O atoms in SB and leaving porous tunnels in CSB. Besides, the yield of the obtained material is upto 25%. The craft process for carbon materials is simple and the original material is low cost. Thereby, it can be found that it is suitable for the industrial production (the inset of **Figure 3a**).

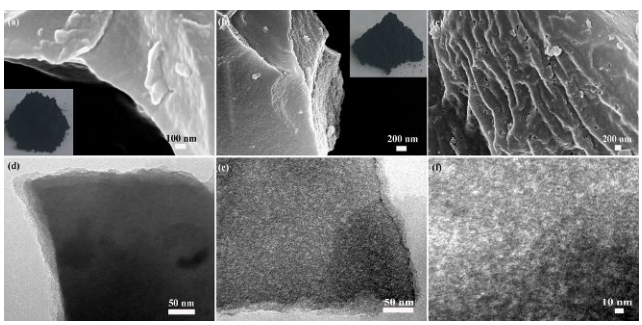

Figure 3. (a) SEM image (the inset is digital photograph of CSB) and (d) TEM image of CSB, (b) SEM image (the inset is digital photograph of ACSB) and (e) TEM image of ACSB in the edge, (c) SEM image and (f) TEM image of ACSB in the middle.

Then, scanning electron microscopy (SEM) and TEM were also employed to investigate the structure of CSB and ACSB. Notably, there is no obvious change of the morphology after the carbonization of SB (**Figure 3a, Figure S1**), which still shows the wrinkled structure. TEM image further demonstrates the plate-like structure of CSB (**Figure 3d**), confirming the laminar structure is still remained. Although CSB maybe exhibit some pores owing to the pyrolysis of SB and the evaporation of H_2O, CO_2 and CO during the carbonization process, the pores are not obvious to find from the typical SEM or TEM images.

As is kown, the high specific surface area benefits the rapid electronic and ionic transport for EDLCs and the large pore volume allows sufficient infiltration of the electrolyte and fast diffusion of lithium ion for LIBs.[41] Thereby, we enhance its specific surface area in the next step. The chemical activation of carbon materials by KOH has been drawn much attention.[42-44] The process for obtaining porous carbon materials is simple, controllable and does not consume expensive reagents. In this work, CSB with KOH is heated at 650 °C for 1 h under nitrogen to obtain ACSB. KOH can be completely transformed to K_2CO_3 at about 600 °C. And K_2CO_3 begins to decompose into CO_2 and K_2O at temperature higher than 700 °C. Therefore, the optimum reaction equation between CSB and KOH in this work is proposed as follow:[45]

$$6KOH + 2C \rightarrow 2K + 3H_2 + 2K_2CO_3 \quad (1)$$

The yield of ACSB is *ca.* 71.3%, which is higher than the carbon yields of *ca.* 36 and 50% in previous reports.[46, 47] After the activation, SEM images of ACSB indicate the laminar structure (**Figure 3b**) and the wrinkled structure (**Figure 3c**) are well remained. Simultaneously, there are abundant pores on the surface of ACSB (**Figure 3c)**, confirming that KOH can effectively create plentiful pores in carbon materials. TEM images demonstrate the existence of the plate-like structure and rich pores in ACSB (**Figure 3e, f**), which correspond with the SEM observation. High-resolution transmission electron microscopy (HRTEM) image further reveals the structure of ACSB, which consists of tiny graphite domains (**Figure S2a**).[48] Besides, the abundant worm-like micropores and mesopores can be clearly observed in **Figure S2b**. The unique pore-size distribution of ACSB could enable fast ion transport and allow sufficient infiltration of the electrolyte for EDLCs and LIBs/SIBs.

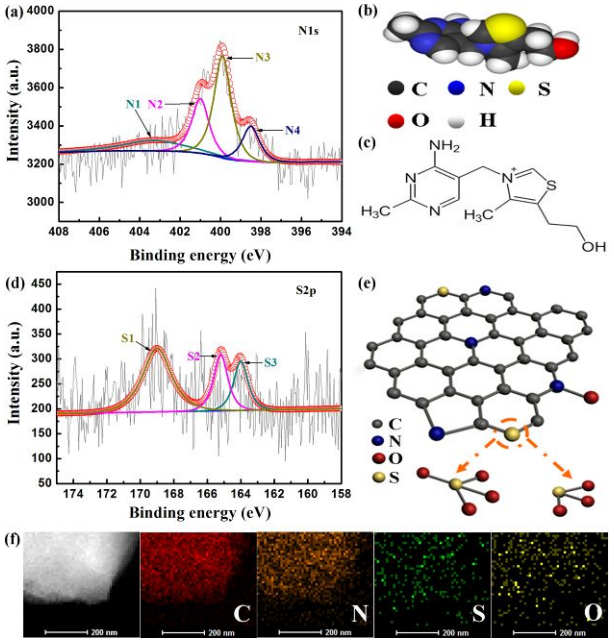

Figure 4. (a) N1s XPS spectra for ACSB (N1: N-oxides of pyridine-N; N2: quaternary-N; N3: pyrrolic-N; N4: pyridinic-N), (b) The structural model and (c) structural formula of thiamine, (d) S2p XPS spectra for ACSB (S1: the oxidised sulfur species; S2: the $S2p_{1/2}$ of –C–S–C–; S3: the $S2p_{3/2}$ of –C–S–C–) and (e) Schematic illustration for chemical structure of ACSB with nitrogen and sulfur dual-doping, (f) STEM image of ACSB and corresponding elemental mapping images of carbon, nitrogen, sulfur and oxygen.

SB contains essential amino-acids and vitamins, which are abundant in nitrogen. Therefore, X-ray photoelectron spectroscopy (XPS) was carried out to detect the differences of nitrogen bonds in CSB and ACSB. The nitrogen peaks of ACSB could be fitted into four peaks (**Figure 4a**).[8, 21] The first peak at 403.3 eV corresponds to N-oxides of pyridine-N (**N1**). The second peak at 401.0 eV may be identified to quaternary-N (**N2**), which is the most stable nitrogen species under the carbonization process of SB and the activation process of CSB. The third peak at 399.9 eV can be attributed to pyrrolic-N (**N3**). The last peak located at 398.5 eV is contributed to the hexagonal pyridinic-N (**N4**). Interestingly, thiamine (**Figure 4b, c**) and some sulfur-containing amino acids are also present in the composition of SB,[49] which result that ACSB is doped with sulfur. The sulfur peaks of ACSB could be fitted into three peaks (**Figure 4d**).[37, 50, 51] The first peak at 168.5 eV should be assigned to the oxidized sulfur species (**S1**), such as the sulfate (–C–SO_4–C–) or sulfonate (–C–SO_3–C–). The other two peaks at 165.2 and 164.0 eV correspond to the $S2p_{1/2}$ (**S2**) and $S2p_{3/2}$ (**S3**) of the –C–S–C– covalent bond, respectively. The presence of nitrogen and sulfur in CSB is similar with ACSB (**Figure S3**). Only carbon, nitrogen, oxygen and sulfur are detected from CSB and ACSB in the range of XPS sensitivity (**Table S1**), indicating the inexistence of other impurities. The amounts of nitrogen and sulfur are 2.2% and 0.97% in CSB and 2.0% and 0.94% in ACSB, respectively. Combining with the XPS spectra and previous report,[12] the possible schematic illustration for chemical structure of ACSB with nitrogen and sulfur dual-doping is shown in **Figure 4e**. Moreover, the elemental mapping images (**Figure 4f**) further demonstrate the uniform distribution of carbon, nitrogen, oxygen and sulfur in ACSB.

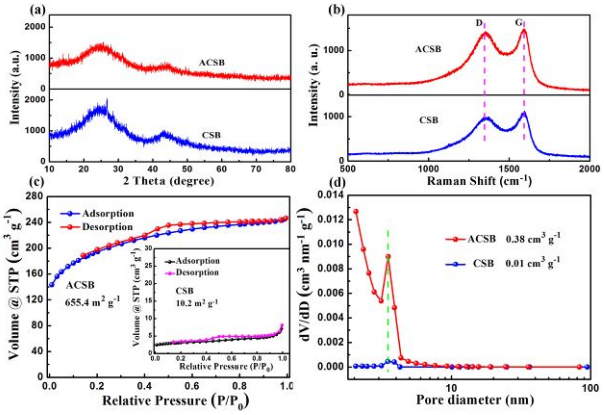

Figure 5. (a) XRD patterns, (b) Raman spectra, (c) N_2 adsorption-desorption isotherms at 77 K and (d) PSD curves of CSB and ACSB. PSD is calculated using the Barrett-Joyner-Halenda (BJH) method.

In the XRD patterns of CSB and ACSB, there are two broad signals around 24° and 44° (**Figure 5a**), which respectively corresponds to the (002) and (100) spacing of the graphene stacks.[52] XRD results indicate that these carbon materials have no impurity, corroborating well with the XPS observation. The presence of trace metals in SB,[49] such as iron, may be in favor of improving the degree of graphitization for CSB and ACSB. The diffraction intensity of the (002) and (100) peak in ACSB is lower than those in CSB under the same condition of detecting, resulting from the chemical activation by KOH to break down the hexagonal symmetry of the graphite lattice and lead to lattice defects in ACSB. The structures of the as-prepared carbon materials were further detected by the Raman spectra. Two strong bands located at around 1355 and 1590 cm^{-1} are assigned to the D-band (D) and the G-band (G),[53] respectively (**Figure 5b**). D could origin from the disorder induced features of carbon and structural defects, owing to the nitrogen, sulfur and oxygen heteroatoms doping in the carbon materials and the chemical activation in ACSB. The increased intensity of D in ACSB also indicates the generation of defects after the chemical activation. Moreover, it could be calculated that the relative intensity ratio of D and G (ID/IG) increases from 0.88 (CSB) to 0.96 (ACSB), showing that the graphitization degree of ACSB decreases. While G corresponds to the sp^2 carbon-bonded graphitic structure, which is beneficial for enhancing the electrical conductivity of carbon materials.[54] Furthermore, the appearance of G indicates the presence of graphitic domains,[55] which is consistent with the HRTEM observation. The obtained carbon materials would be in favor of improving electrical conductivity when used as electrode materials of the energy storage devices.

N_2 adsorption/desorption isotherms and corresponding pore size distribution (PSD) curves for CSB and ACSB are collected (**Figure 5c**, **Figure 5d**). The specific surface area and PSD are calculated using the Brunauer-Emmett-Teller (BET) method and Barrett-Joyner-Halenda (BJH) method, respectively. The isotherms of ACSB are typical type I and type IV isotherms with a hysteresis loop, indicating the presence of micropores and mesopores.[56] In detail, the isotherms have a clear uptrend at the low relative pressure (P/P_0<0.4), manifesting that ACSB is rich in micropores. The appearance of significant hysteresis

characteristics at high relative pressure (P/P_0=0.4-0.8) in the isotherms demonstrates the existence of abundant mesopores. Therefore, ACSB exhibits a highly developed hierarchical porosity network of micropores in combination with mesopores. While the isotherms of CSB are typical type IV isotherms with a hysteresis loop (the inset of **Figure 5c**), indicating the presence of mesopores. Meanwhile, a slight upward tendency at the high relative pressure (P/P_0=0.95-1.0) corresponds to the presence of macropores, resulting from the accumulation of carbon particles. The PSD data indicates the size of the majority of pores is about 3 nm in CSB and ACSB. A clear upward trend peak (<2 nm) further confirms the abundant micropores in ACSB. The chemical activation effectively creates abundant pores, making the specific surface area from 10.2 to 655.4 m^2 g^{-1} and the total pore volume from 0.01 to 0.38 cm^3 g^{-1} (**Table S4**).

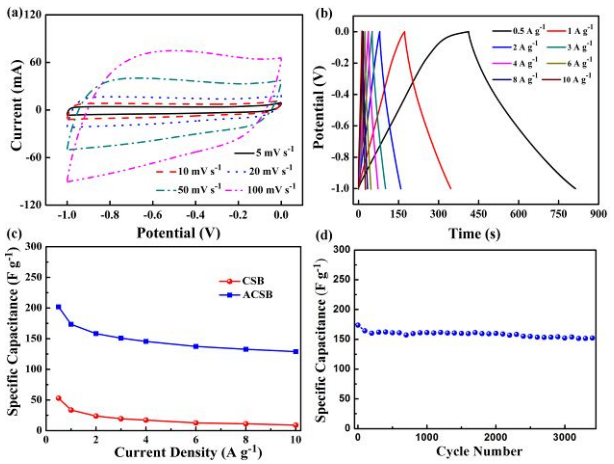

Figure 6. CV curves of the ACSB electrode in 6 M KOH aqueous solution at different scan rates, (b) The galvanostatic charge-discharge curves of the ACSB electrode at different current densities, (c) The specific capacitances calculated from the discharge curves under different current densities, (d) Cyclic stability of the ACSB-based EDLCs at a current density of 1 A g^{-1}.

Cyclic voltammetry (CV) and galvanostatic charge/discharge measurements in a three-electrode system were carried out to investigate the electrochemical performance of CSB and ACSB as electrode materials for EDLCs. The regular rectangular shapes are present at low scan rates, which is the typical characteristic of EDLCs. The approximately rectangular shape of the CV curve can still be maintained even when the scan rate is as high as 100 mV s^{-1} (**Figure 6a**), indicating the rapid ion transport can be operated in ACSB. The galvanostatic charge/discharge curves of the ACSB electrode at different current densities show almost isosceles triangular shapes (**Figure 6b**), demonstrating the ideal charge and discharge characteristics for EDLCs. Although CSB has a low specific surface area, the sulfur and nitrogen doping could increase the specific capacitance (**Figure S4**). The incorporation of sulfur in carbon materials can increase the space utilization by a specific electrosorption of electrolyte ions and contribute to pseudocapacitance.[35] The incorporation of nitrogen in carbon materials can increase the electrical conductivity, wettability, and contribute to a pseudocapacitive effect.[44] CSB has specific capacitances of 53 F g^{-1} at a current density of 0.5 A g^{-1} and 34 F g^{-1} at 1 A g^{-1} (**Table S5**), which is marginally higher than the previous reports of the 100% CNT film (24 F g^{-1}) and the pristine CNT paper (32 F g^{-1}).[57, 58] After the KOH activation, the hierarchically porous structure in ACSB could be favor of fast electron and ion transport (**Figure S5**). Therefore, ACSB exhibits a high specific capacitance of 202 F g^{-1} at 0.5 A g^{-1}. Even at a current density of 10 A g^{-1}, the specific capacitance is still upto 129 F g^{-1}, which is higher than the results of previous reports (**Table S6**). Moreover, ACSB exhibits a superior rate performance as shown in **Figure 6c**. Simultaneously, the retention of specific capacitance for the ACSB electrode is close to 90% after 3000 cycles (**Figure 6d**), showing it presents an excellent cycling stability. In addition, ACSB delivers a high specific capacitance of 229 F g^{-1} at a current density of 0.5 A g^{-1} in 1 M H_2SO_4 (**Figure S6**), which is higher than the specific capacitances of GO/CNT hybrid powder (180 F g^{-1} at 0.4 A g^{-1}) and 66.7wt% CNTs (*ca.* 180 F g^{-1} at 0.5 A g^{-1}) in previous reports.[57, 59]

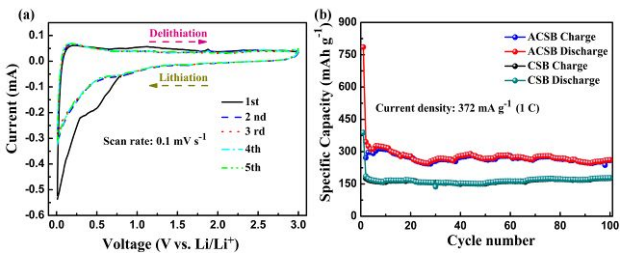

Figure 7. (a) Typical CV curves of the ACSB anode for LIBs at a scan rate of 0.1 mV s^{-1}, (b) Cycling performance of the CSB and ACSB anodes for LIBs at a constant rate of 1 C (1 C=372 mA g^{-1}).

Inspired by the commercialization of graphite as anode for LIBs, we assemble CR2032-type coin cells to estimate the electrochemical performance of CSB and ACSB electrodes. There is no an obvious change after the first cycle in the CV curves of the ACSB electrode (**Figure 7a**), displaying superior reactive reversibility and cycling stability for LIBs. The initial discharge capacities of CSB and ACSB are respectively 467.1 and 845.2 mAh g^{-1} at a current rate of 0.5 C (**Figure S7**). Simultaneously, the two anode materials reveal good cycling performance after the first cycle, which agree well with the CV curves. Even at a current rate of 1 C, the discharge capacity of CSB is still 178.1 mAh g^{-1} and the discharge capacity of ACSB is upto 261.5 mAh g^{-1} after 100 cycles (**Figure 7b**), which are superior to the 3D MWCNTs-graphene-PET (~100 mAh g^{-1} at 316 mA g^{-1})[28] and graphite (~150 mAh g^{-1} at 300 mA g^{-1}).[29] The favorable electrochemical performance of the CSB anode could be attributed to the dual-doping of sulfur and nitrogen. The further improvement of the electrochemical performance for the ACSB anode is benefited from the hierarchically porous structure and the dual doping of sulfur and nitrogen. The porous structure of ACSB could allow sufficient infiltration of the electrolyte and shorten the transport pathway for both electron and ion (**Figure S8**).

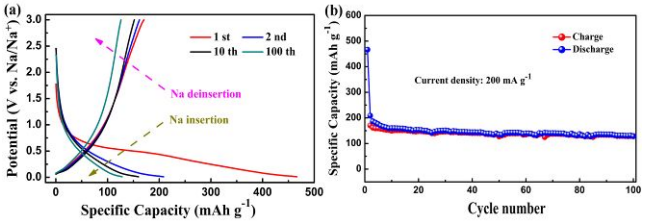

Figure 8. (a) Galvanostatic charge/discharge profiles and (b) Cycling performance of the ACSB anode for SIBs at a current density of 200 mA g^{-1}.

Recently, SIBs have been paid worldwide attention due to the abundant storage and low cost of sodium.[60-62] When the ACSB electrode is estimated as the anode material for SIBs, the initial discharge capacity is 466.3 mAh g^{-1} at a current density of 200 mA g^{-1} (**Figure 8a**). The irreversible capacity loss occurred during the first cycle results from the electrolyte decomposition to form a solid-electrolyte interphase (SEI) layer on the surface of electrodes.[63] The galvanostatic charge/discharge profiles of the ACSB electrode are similar with the previous reports, representing the insertion/deinsertion of sodium in ACSB.[39, 64] As shown in **Figure 8b**, the ACSB electrode shows outstanding cycling performance, which is superior to the AG and CMFs electrodes,[39, 48] demonstrateing that the as-prepred materials have great potential in the applications of SIBs.

Conclusions

In summary, the sulfur and nitrogen dual-doping porous carbon materials have been successfully prepared from the shell of broad beans and applied for EDLCs, LIBs and SIBs. The specific capacitance is upto 129 F g^{-1} for EDLCs at a high current density of 10 A g^{-1}; the discharge capacity at a current rate of 1 C still remains at 261.5 mAh g^{-1} for LIBs after 100 cycles; and the initial discharge capacity is as high as 466.3 mAh g^{-1} for SIBs at a current density of 200 mA g^{-1}. These electrochemical results clearly prove ACSB to be a promising candidate for energy storage applications. Based on this research, the activating agent species (water vapor, $ZnCl_2$, and H_3PO_4) and weight ratio of activating agents to carbon precursors should be specially tailored to obtain the optimal porous carbon materials for different energy storage devices, such as lithium-air batteries, lithium-sulfur batteries and photocatalysis.

Acknowledgements

The authors are grateful to the National Key Basic Research Program 973 (No. 2014CB239701), National Natural Science Foundation of China (No. 21173120, No. 51372116), Natural Science Foundation of Jiangsu Province (No. BK2011030). G. Y. Xu and B. Ding would like to thank Funding of Graduate Innovation Center in NUAA (No. Kfjj20130219), Jiangsu Innovation Program for Graduate Education (CXZZ13_0158) and Outstanding Doctoral Dissertation in NUAA (BCXJ13-13).

Notes and references

Jiangsu Key Laboratory of Material and Technology for Energy Conversion, College of Material Science and Engineering, Nanjing University of Aeronautics and Astronautics, Nanjing, 210016, P. R. China
Fax: +86-025-52112626; Tel: +86-025-52112626;
E-mail: azhangxg@163.com

† Electronic Supplementary Information (ESI) available: [The Supporting Information contains descriptions of preparation methods for CSB and ACSB, as well as structural and electrochemical characterization methods of these materials.] See DOI: 10.1039/b000000x/

1. N. Liu, K. Huo, M. T. McDowell, J. Zhao and Y. Cui, *Sci. Rep.*, 2013, **3**, 1919.
2. L. Y. Zhang, Y. Y. Wang, B. Peng, W. T. Yu, H. Y. Wang, T. Wang, B. W. Deng, L. Y. Chai, K. Zhang and J. X. Wang, *Green Chem.*, 2014, **16**, 3926-3934.
3. X. Wang, G. Liu, Q. Ou, X. Zhao, J. Hao and X. Zhou, *Asian Agricultural Research*, 2013, **5**, 111-113.
4. M. Zhong, E. K. Kim, J. P. McGann, S. E. Chun, J. F. Whitacre, M. Jaroniec, K. Matyjaszewski and T. Kowalewski, *J. Am. Chem. Soc.*, 2012, **134**, 14846-14857.
5. S. Yang, L. Zhi, K. Tang, X. Feng, J. Maier and K. Müllen, *Adv. Funct. Mater.*, 2012, **22**, 3634-3640.
6. Y. Wang, Y. Shao, D. W. Matson, J. Li and Y. Lin, *ACS Nano*, 2010, **4**, 1790-1798.
7. Y. Dong, H. Pang, H. B. Yang, C. Guo, J. Shao, Y. Chi, C. M. Li and T. Yu, *Angew. Chem. Int. Ed.*, 2013, **52**, 7800-7804.
8. L. Qie, W. M. Chen, Z. H. Wang, Q. G. Shao, X. Li, L. X. Yuan, X. L. Hu, W. X. Zhang and Y. H. Huang, *Adv. Mater.*, 2012, **24**, 2047-2050.
9. J. P. Paraknowitsch and A. Thomas, *Energy Environ. Sci.*, 2013, **6**, 2839-2855.
10. L. F. Chen, Z. H. Huang, H. W. Liang, Q. F. Guan and S. H. Yu, *Adv. Mater.*, 2013, **25**, 4746-4752.
11. L. F. Chen, X. D. Zhang, H. W. Liang, M. Kong, Q. F. Guan, P. Chen, Z. Y. Wu and S. H. Yu, *ACS Nano*, 2012, **6**, 7092-7102.
12. J. Liang, Y. Jiao, M. Jaroniec and S. Z. Qiao, *Angew. Chem. Int. Ed.*, 2012, **51**, 11496-11500.
13. P. Zhang, Y. Gong, H. Li, Z. Chen and Y. Wang, *Nat. Commun.*, 2013, **4**, 1593.
14. P. G. Bruce, S. A. Freunberger, L. J. Hardwick and J. M. Tarascon, *Nat. Mater.*, 2012, **11**, 19-29.
15. C. Merlet, B. Rotenberg, P. A. Madden, P. L. Taberna, P. Simon, Y. Gogotsi and M. Salanne, *Nat. Mater.*, 2012, **11**, 306-310.
16. H. Jiang, P. S. Lee and C. Li, *Energy Environ. Sci.*, 2013, **6**, 41-53.
17. Y. Li, Z. Y. Fu and B. L. Su, *Adv. Funct. Mater.*, 2012, **22**, 4634-4667.
18. L. Yin, J. Wang, F. Lin, J. Yang and Y. Nuli, *Energy Environ. Sci.*, 2012, **5**, 6966-6972.
19. D. R. MacFarlane, N. Tachikawa, M. Forsyth, J. M. Pringle, P. C. Howlett, G. D. Elliott, J. H. Davis, M. Watanabe, P. Simon and C. A. Angell, *Energy Environ. Sci.*, 2014, **7**, 232-250.
20. D. W. Su, S. X. Dou and G. X. Wang, *J. Mater. Chem. A*, 2014, **2**, 11185-11194.
21. G. Xu, B. Ding, P. Nie, L. Shen, J. Wang and X. Zhang, *Chem. Eur. J.*, 2013, **19**, 12306-12312.
22. S. Wang, R. Liu, C. Han, J. Wang, M. Li, J. Yao, H. Li and Y. Wang, *Nanoscale*, 2014, **6**, 13510-13517.
23. Y. Gong, Z. Wei, J. Wang, P. Zhang, H. Li and Y. Wang, *Sci. Rep.*, 2014, **4**, 6349.
24. Q. Li, R. Jiang, Y. Dou, Z. Wu, T. Huang, D. Feng, J. Yang, A. Yu and D. Zhao, *Carbon*, 2011, **49**, 1248-1257.
25. Y. Yoon, K. Lee, C. Baik, H. Yoo, M. Min, Y. Park, S. M. Lee and H. Lee, *Adv. Mater.*, 2013, **25**, 4437-4444.
26. J. H. Lee, N. Park, B. G. Kim, D. S. Jung, K. Im, J. Hur and J. W. Choi, *ACS Nano*, 2013, **7**, 9366-9374.
27. T. M. Arruda, M. Heon, V. Presser, P. C. Hillesheim, S. Dai, Y. Gogotsi, S. V. Kalinin and N. Balke, *Energy Environ. Sci.*, 2013, **6**, 225-231.
28. C. Kang, R. Baskaran, J. Hwang, B. C. Ku and W. Choi, *Carbon*, 2014, **68**, 493-500.
29. M. S. Kim, B. Fang, J. H. Kim, D. Yang, Y. K. Kim, T. S. Bae and J. S. Yu, *J. Mater. Chem.*, 2011, **21**, 19362-19367.
30. K. Tang, R. J. White, X. Mu, M. M. Titirici, P. A. van Aken and J. Maier, *ChemSusChem*, 2012, **5**, 400-403.
31. W. Li and D. Zhao, *Chem. Comm.*, 2013, **49**, 943-946.

32. Y. Fang, D. Gu, Y. Zou, Z. Wu, F. Li, R. Che, Y. Deng, B. Tu and D. Zhao, *Angew. Chem. Int. Ed.*, 2010, **49**, 7987-7991.
33. Y. Wang and Y. Xia, *Adv. Mater.*, 2013, **25**, 5336-5342.
34. Z. Liu, H. Nie, Z. Yang, J. Zhang, Z. Jin, Y. Lu, Z. Xiao and S. Huang, *Nanoscale*, 2013, **5**, 3283-3288.
35. M. Seredych and T. J. Bandosz, *J. Mater. Chem. A*, 2013, **1**, 11717-11727.
36. L. Wei, M. Sevilla, A. B. Fuertes, R. Mokaya and G. Yushin, *Adv. Funct. Mater.*, 2012, **22**, 827-834.
37. Y. Yan, Y. X. Yin, S. Xin, Y. G. Guo and L. J. Wan, *Chem. Comm.*, 2012, **48**, 10663-10665.
38. Y. Mao, H. Duan, B. Xu, L. Zhang, Y. Hu, C. Zhao, Z. Wang, L. Chen and Y. Yang, *Energy Environ. Sci.*, 2012, **5**, 7950-7955.
39. H. G. Wang, Z. Wu , F. L. Meng , D. L. Ma , X. L. Huang , L. M. Wang and X. B. Zhang, *ChemSusChem*, 2013, **6**, 56-60.
40. N. W. Li, M. B. Zheng, H. L. Lu, Z. B. Hu, C. F. Shen, X. F. Chang, G. B. Ji, J. M. Cao and Y. Shi, *Chem. Comm.*, 2012, **48**, 4106-4108.
41. G. Xu, B. Ding, L. Shen, P. Nie, J. Han and X. Zhang, *J. Mater. Chem. A*, 2013, **1**, 4490-4496.
42. Y. Zhu, S. Murali, M. D. Stoller, K. J. Ganesh, W. Cai, P. J. Ferreira, A. Pirkle, R. M. Wallace, K. A. Cychosz, M. Thommes, D. Su, E. A. Stach and R. S. Ruoff, *Science*, 2011, **332**, 1537-1541.
43. L. Zhang, F. Zhang, X. Yang, G. Long, Y. Wu, T. Zhang, K. Leng, Y. Huang, Y. Ma, A. Yu and Y. Chen, *Sci. Rep.*, 2013, **3**, 1408.
44. J. Wei, D. Zhou, Z. Sun, Y. Deng, Y. Xia and D. Zhao, *Adv. Funct. Mater.*, 2013, **23**, 2322-2328.
45. J. Wang and S. Kaskel, *J. Mater. Chem.*, 2012, **22**, 23710-23725.
46. D. Huličová, K. Hosoi, S. I. Kuroda, H. Abe and A. Oya, *Adv. Mater.*, 2002, **14**, 452-455.
47. D. Hulicova, F. Sato, K. Okabe, M. Koishi and A. Oya, *Carbon*, 2001, **39**, 1438-1442.
48. W. Luo, J. Schardt, C. Bommier, B. Wang, J. Razink, J. Simonsen and X. Ji, *J. Mater. Chem. A*, 2013, **1**, 10662-10666.
49. Wikipedia,*http://en.wikipedia.org/wiki/Vicia_faba#Other_uses*, 2014.
50. F. Bottger-Hiller, A. Mehner, S. Anders, L. Kroll, G. Cox, F. Simon and S. Spange, *Chem. Comm.*, 2012, **48**, 10568-10570.
51. J. P. Paraknowitsch, A. Thomas and J. Schmidt, *Chem. Comm.*, 2011, **47**, 8283-8285.
52. G. Xu, B. Ding, P. Nie, L. Shen, H. Dou and X. Zhang, *ACS Appl. Mater. Interfaces*, 2013, **6**, 194-199.
53. X. Xu, Y. Li, Y. Gong, P. Zhang, H. Li and Y. Wang, *J. Am. Chem. Soc.*, 2012, **134**, 16987-16990.
54. K. Ai, Y. Liu, C. Ruan, L. Lu and G. Lu, *Adv. Mater.*, 2013, **25**, 998-1003.
55. R. Jia, J. Chen, J. Zhao, J. Zheng, C. Song, L. Li and Z. Zhu, *J. Mater. Chem.*, 2010, **20**, 10829-10834.
56. Y. S. Su and A. Manthiram, *Nat. Commun.*, 2012, **3**, 1166.
57. Z. D. Huang, B. Zhang, S. W. Oh, Q. B. Zheng, X. Y. Lin, N. Yousefi and J. K. Kim, *J. Mater. Chem.*, 2012, **22**, 3591-3599.
58. S. L. Chou, J. Z. Wang, S. Y. Chew, H. K. Liu and S. X. Dou, *Electrochem. Commun.*, 2008, **10**, 1724-1727.
59. S. H. Aboutalebi, A. T. Chidembo, M. Salari, K. Konstantinov, D. Wexler, H. K. Liu and S. X. Dou, *Energy Environ. Sci.*, 2011, **4**, 1855-1865.
60. H. Zhu, Z. Jia, Y. Chen, N. Weadock, J. Wan, O. Vaaland, X. Han, T. Li and L. Hu, *Nano Lett.*, 2013, **13**, 3093-3100.
61. X. Yu, H. Pan, W. Wan, C. Ma, J. Bai, Q. Meng, S. N. Ehrlich, Y. S. Hu and X. Q. Yang, *Nano Lett.*, 2013, **13**, 4721-4727.
62. P. Nie, L. Shen, H. Luo, B. Ding, G. Xu, J. Wang and X. Zhang, *J. Mater. Chem. A*, 2014, **2**, 5852-5857.
63. K. T. Lee, R. Black, T. Yim, X. Ji and L. F. Nazar, *Adv. Energy Mater.*, 2012, **2**, 1490-1496.
64. S. Komaba, W. Murata, T. Ishikawa, N. Yabuuchi, T. Ozeki, T. Nakayama, A. Ogata, K. Gotoh and K. Fujiwara, *Adv. Funct. Mater.*, 2011, **21**, 3859-3867.

TOC figures

Biomass-derived porous carbon material with sulfur and nitrogen dual-doping exhibits great potential for energy storage devices.